Analysis Upwelling changes using Wavelet Transform

Xuweiyi Chen, Zhengyang Xu

Abstract

Upwelling is one of most important aspects of ocean dynamics. Wavelet Analysis is an effective tool to understand cycles in time series. With multiple detrend methods, we can quantify annual and intra-annual cycles and provide visualizations for upwelling changes across time. We utilized a data processing pipeline studied upwelling changes in Peruvian, Moroccan and Chilean coast and extended this method to other regions. We found correlations between upelling changes after 2010 between Peruvian system and Morocco system. Our result supports part of the Bakun hypothesis and recognize the complexity of ocean mechanisms due to inconsistent findings with Bakun hypothesis, especially equatorward migration and the absence of homogenization of the upwelling in Morocco.

1. Introduction and Preliminary

Ocean has always been a complex system. Upwelling is one of the key perspective of how people try to understand the ocean.In general, upwelling defines as an upward movement of water parcels in the water column that is maintained over a reasonable long period (several days to weeks), long enough to life water parcels over a vertical distance of 100 m or more (Kaempf and Chapman, 2016). There are three main forms of wind-driven upwelling are (i) coastal upwelling, (ii) equatorial upwelling, and (iii) ice-edge upwelling. Some upwelling systems, such as the world's largest upwelling regions found off Peru/Chile, California, Northwest Africa, and southwest Africa, exhibit nutrient-rich undercurrents at shelf-break depth acting as both a source for upwelled water and as a nutrient trap (Montecino and Lange, 2009). As Bakun stated (Bakun et al., 2015), upwelling changes can affect the ocean in many perspectives. One of the most important perspective is the fish industry which upwelling can bring nutrients-rich water from bottom of the ocean to the top of the ocean.

However, in a recent article discussing the effects of greenhouse gas, Bakun hypothesized that some mechanisms involving greenhouse-associated intensification of thermal low-pressure cells over the coastal landmasses of upwelling regions suggest general intensification of wind-driven ocean upwelling in coastal upwelling regions of the world's oceans (Bakun et al., 2010). At the year of 2010, Bakun was puzzled by the upwelling process in the Peru system might be weaken due to empirical results. As a look back, we found that the upwelling process in Peru system has been intensified.

In this article, we want to first introduce the intensification mechanism and take a closer look at Peruvian and Chilean coast. For many of paper discussing upwelling, it fails to provide us how they process and extract features from the original data. We want to fully introduce our data processing pipeline based

on wavelet analysis and discuss our results.

1.1. Intensification Mechanism

One of the main arguments that Bakun made for Upwelling intensification is water has much higher specific heat capacity compared to land. (Bakun et al., 2010) For most of the world's oceans, coastal upwelling operate mostly during warm seasons. Due to the fact that water has much higher specific heat capacity compared to land, air temperature over a coastal landmass are typically higher compared to the air temperature over adjacent sea. This cross-shore pressure will drive an offshore-directed Ekman transport of surface water. While the greenhouse gas concentration increases in the atmosphere, land will heat even faster compared to the ocean. As a consequence, the coastal wind will be intensified and the intensity of upwelling will be extended.

1.2. Upwelling at Peruvian and Chilean Coast

The Peru-Chile upwelling system is one of the most productive ecosystems on Earth. The scientific understanding of the physics, ecosystem dynamics and carbon cycle of this particular region has been pivotal in the progress of the climate sciences. As an example, the irregular disppearance of upwelling-enhaned productivity in the region, originally refered to by fisherman as El Nino, has led to the discovery of the El Nino Southern Oscillation (ENSO) which is one of the leading modes of global climate variability. There have been a lot research concerning the upwelling system at Peruvian and Chilean. Along the coasts of Peru and northern and central Chile, upwelling is localized and its occurrence changes changes from being mostly continuous in Peru and northern Chile to a more seasonal pattern in southern-central Chile. Along the Chilean coast, four regions are recognized for especially strong upwelling. Based on (Figueroa and Moffat, 2000) and (Arias-Pérez and Tavera-Mesías, 2015). Regional upwelling centres are found at

1. Antofagasta and Mejillones Peninsula (23 S)
2. Coquimbo Bay (30 S)
3. Valparaiso (33 S) and
4. Bay of Concepcion (37 S)

Since we just discussed the intensification mechanism in the previous section, we want to take this consideration for Peruvian and Chilean upwelling system. In the case of Peru, the low latitude situation results in upwelling-favorable winds year round, with a wintertime strengthening of the anticyclonic subtropical high offshore producing a seasonal strengthening of the pressure gradient. In one of the eariler paper from Bakun, the upwelling system off Peru presents an extreme tropical case; coastal upwelling continues throughout the year and is actually somewhat more intense in austral winter than

in summer. Because of the low-latitude location and correspondingly weakened geostrophic constraint, upwelling index computations are not appropriate. It also stated that the long-term incresing trend in equatorward alongshore wind stress is not only clearly evident during the spring to summer half of the year, but also during fall to winter.

In majority of the previous research, Peru is one of the good example that its upwelling has been intensified (Bakun, 1990).

In the scope of this discussion, we followed the above by dividing the Peruvian and Chilean into three regions. At 15 S, upwelling-favourable alongshore winds are a largely continuous phenomenon. Interestingly, the time series indicates climate shifts of surface wind systems and the associated magnitude of the upwelling index.At 21 S, weak but continuous upwelling-favourable winds occurred until 1996, followed by a transition to a regime of markedly reduced alongshore winds. In this region, we can clearly identify ENSO-related wind disturbances. Noted that we could see the upwelling has been affected by the strong 1982/83 and 1998/99 El Nino events. The upwelling dynamics off the northern portion of Chile have a pronounced seasonal cycle. Upwelling-favourable winds develop regularly during austral summer, but tend to vanish during ausstral winter. Thus, the Peruvian and Chilean upwelling system is not only aseasonal but should be view from different perspectives.

2. Methods and Results

2.1. Data

For the analysis upwelling systems, we utilized the time series of monthly mean upwelling index at various locations along the coasts of Peru and Chile for the period 1 January 1981 to 31/12/2020, and of Morocco for the period from 15 July 1982 to 15 July 2022 from the monthly global Ekman transport indices on a 1-degree grid by Environmental Research Division (ERD). https://oceanview.pfeg.noaa.gov/products/upwelling/bakun. Based upon Ekman's theory, the mass transfer of surface water caused by wind stress is 90 degrees to the right of the wind direction under steady condition. To calculate upwelling index, we rotated Ekman transport to find the offshore component using the geometry of the coastline. Specifically, we used monthly ektrx (East-West Component of Ekman Transport), ektry (North-South Component of Ekman Transport) , and coastline orientation, following the python code in Appendix.

2.2. Wavelet Analysis

Wavelet analysis is becoming a common tool for analyzing localized variations of power within a time series. By decomposing a time series into time-frequency space, one is able to determine both the dominant modes of variability and how those modes vary in time. The wavelet transform has been

widely used for numerous studies. A wavelet transform can be represented as the following:

$$CWT_x^{\psi}(\tau, s) = \Psi_x^{\psi}(\tau, s) = \frac{1}{\sqrt{|s|}} \int x(t)\psi^* \left(\frac{t-\tau}{s}\right) dt$$

where τ denotes the translation, and s is the scale parameter. $\psi(t)$ is the transforming function, and it is called the mother wavelet. We recommend (A Practical Guide to Wavelet Analysis) since it offer a complete and easy-to-use wavelet analysis toolkit, including statistical significance testing, which elevates the use of wavelet analysis from qualitative analysis to quantities analysis.

In the following discussion of wavelet analysis, we want to borrow the ideas from (Climate Signal Detection Using Wavelet Transform: How to make a Time Series Sing). We want to show four different scenarios of wavelet analysis and present their difference and its implication from the perspective of analysing upwelling system.

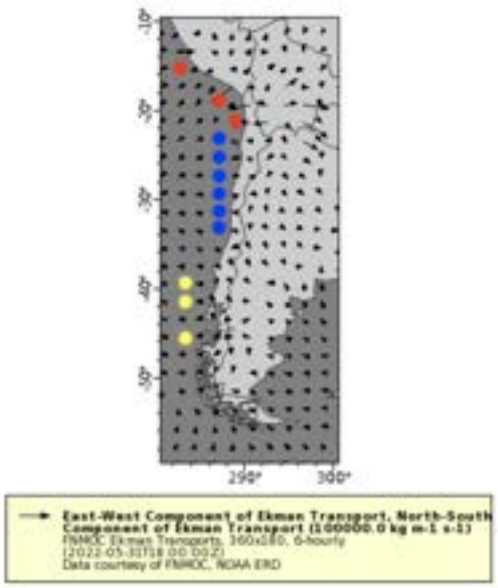

Figure 1. This plot demonstrate the data points we utilized for wavelet analysis. Different colors indicate different regions.

2.2.1. Analysis of Moroccan Upwelling

We firstly normalized monthly upwelling data on Moroccan coast from 1982 to 2022. To better study the cyclical trend of upwelling, we remove the overall trend of data by difference. In other words, we represented each data point by its difference between itself and previous one. Afterwards, we used morlet wavelet as the mother wavelet, and scale between 0.0625 to 64 for the wavelet analysis. In addition, we adopt the cumulative moving average, where we take the unweighted mean of all the observations up to the time of calculation, to study the general trend of upwelling.

$$CMA_t = \frac{x_1 + x_2 + x_3 + ... + x_t}{t}$$

Output as following:

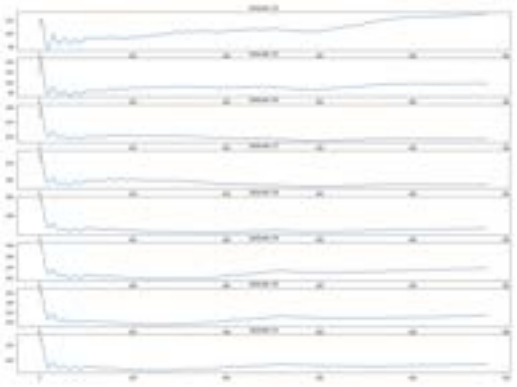

Figure 2. Cumulative moving average

From 1982 to 2022, most of the Ekman transport indices are positive values indicates that the Moroccan area experiences a year-round upwelling. In addition, the upwelling shows a noticeable seasonality. The minimum values of the upwelling system occur in the winter season, and it peaks during summer.(Ismail et al., 2017) Bakun hypothesized that the upwelling system would increase on global scale due to global warming, basing on the data collected before 1985. The differential heating causes the land-sea pressure gradient to increase, which in turn strengthens the winds that are conducive for upwelling. (Narayan et al., 2010) In our study of the Moroccan area, in lower latitudes from 24 to 27 degrees, the upwelling system intensified significantly after 2010, while the upwelling system showed a sharp increase around 2003 in higher latitudes from 28 to 31 degrees. As shown in Fig. 2, our outcomes are consistent with Bakun's hypothesis in terms of the general increase of upwelling, but we also notice the upwelling system is very location dependent. Namely, the trends vary significantly along the latitudes.

Furthermore, Bakun suggested that the upwelling system would shift poleward through the 21st century (Rykaczewski et al., 2015). This predicted rise in upwelling intensity and duration at high latitudes and lack of such increase at lower latitudes will cause a notable reduction of the latitudinal variation in coastal upwelling. However, in fact the Moroccan upwelling system at higher latitudes intensified around

2003 prior to lower latitudes increased after 2010, which indicates the upwelling shifts equatorward. Consequently, the substantial difference intensification time between higher latitude and lower latitudes result in two increase of heterogeneity. This result can be proved by spatial standard deviation, which we defined as $s = \sqrt{\sum_i^N (Y_i - \widehat{y})^2 (N-1)}$, where $\widehat{Y}$ is the mean value of upwelling intensity over all latitudes, Y_i is the value of the upwelling intensity at latitude i, and N is the number of latitudes. Large and small value of s indicate weak homogenization and, respectively, strong homogenization. (Wang et al., 2015) as shown in Fig. 25

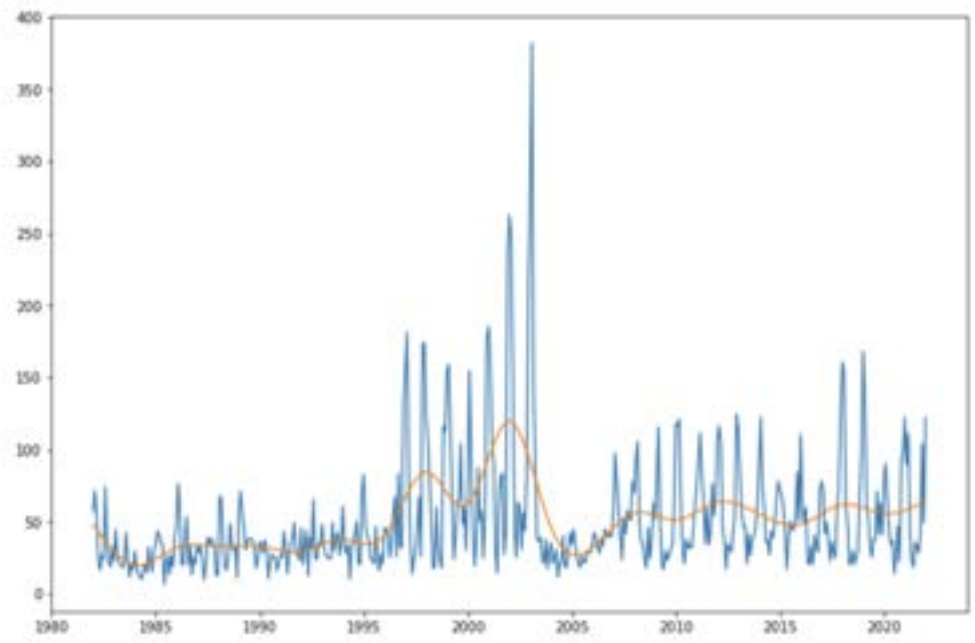

Figure 3. Morocco homogenization

The outcomes of the wavelet transform are shown in Fig. 4. In this graph, red color represents a strong cycle, while blue color refers to a weak cycle. From the graph, we can observe a consistent and remarkable cycle, ranging from 0.8 years to 1.2 years. In contrast, strength in sub-yearly cycle varies irregularly. For example, at latitude 30, the sub-yearly cycle was rarely observed from 1989 to 1993, while it was significant around 2003. For cycles less than one year, the only thing we found is a weak 4-month cycle appears in the Moroccan coastal and the intensity of sub-yearly cycle usually varies with the intensity of one year cycle. In the future study, we suggest finding a better way to deal with the power of cycles that are not exactly one year. For example, future researchers could sum over the power of cycles within one year.

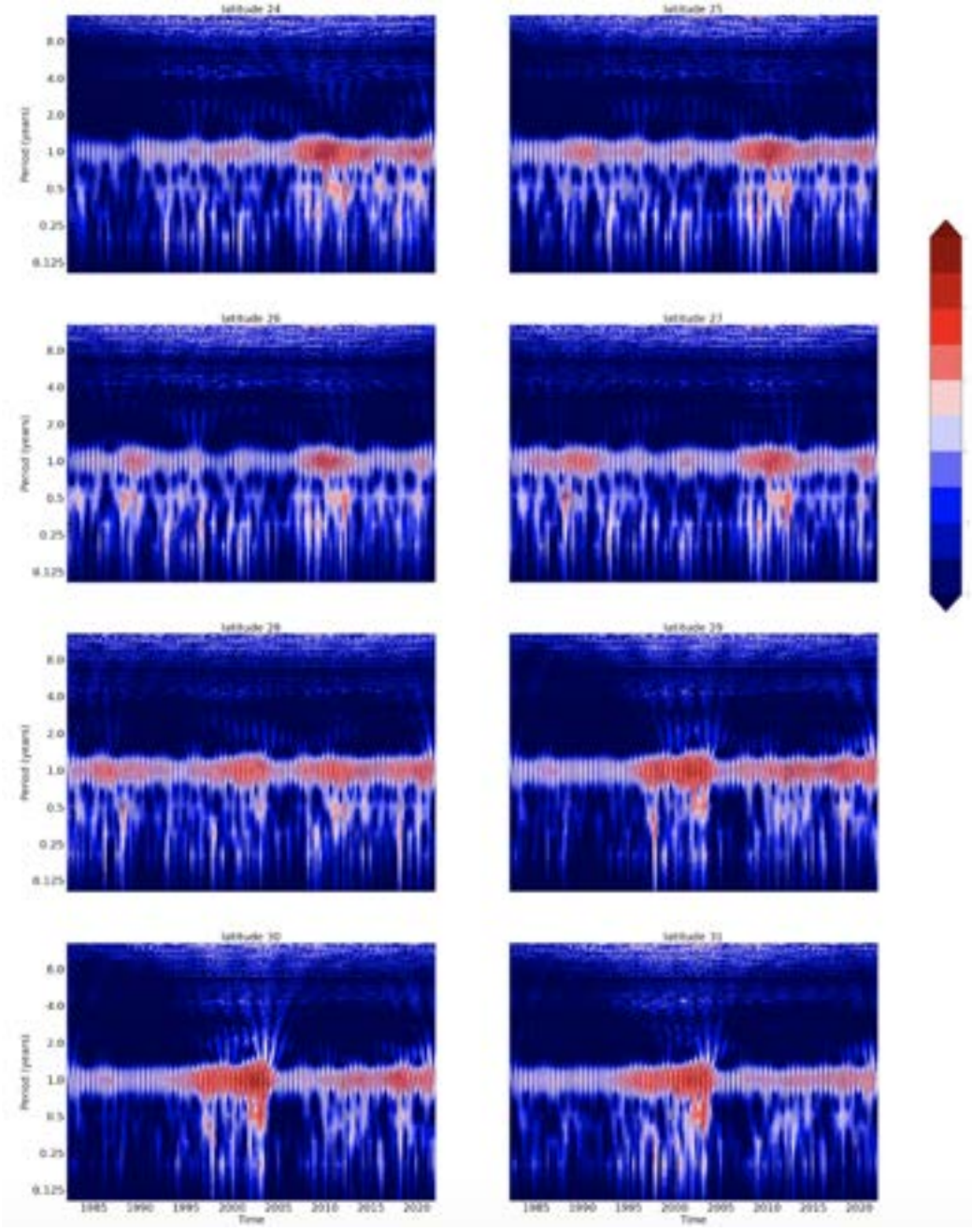

Figure 4. Morocco wavelet analysis

2.2.2. AMPLITUDE MODULATION

We define amplitude modulation as

$$s(t) = A(1 + \alpha \cos \Omega t) \cos \omega t \tag{1}$$

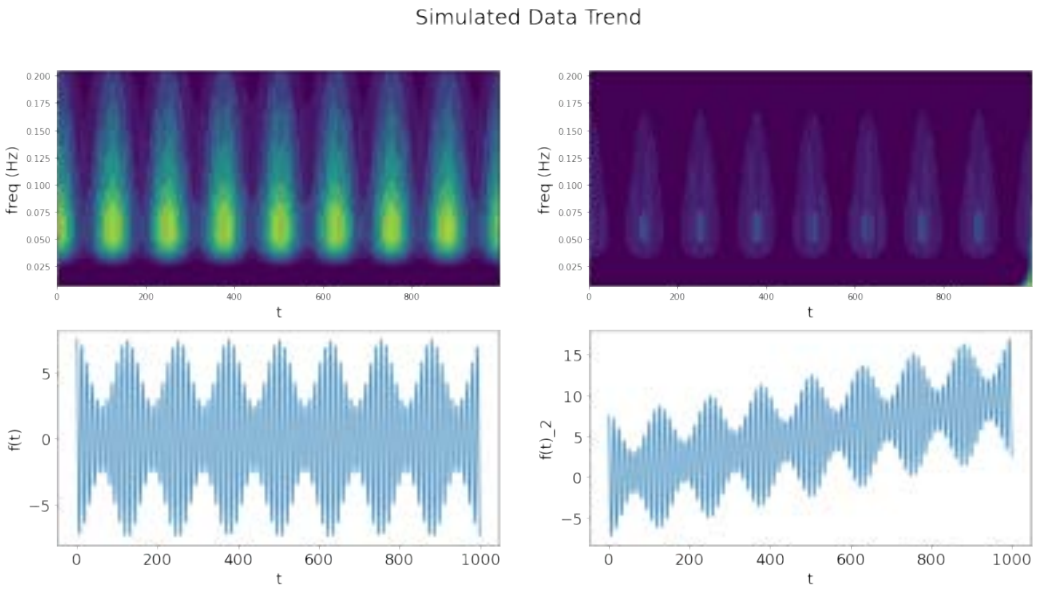

Figure 5. The left two images demonstrate amplitude modulation without trend and the right two images demonstrate amplitude modulation with a linear trend.

The amplitude modulation signal 1 can be often found in a climate system involving nonlinear interactions between different scales or interference of a frequency component. Note in the 5, we have a comparison between two simulated data trends. The left side is a stream of simulation data with no bias and the right side is a stream of simulation data with trend. We could easily see that the corresponding wavelet transform are dramatically different. This shape of wavelet transform can be interpreted as amplitude modulation.

There are more discussions about amplitude modulation related to the next section. We will be able to detect amplitude shift in the time series using wavelet transform. The dark portion between two adjacent light sections are one of the representations for lower amplitude.

2.2.3. FREQUENCY MODULATION

We define frequency modulation as

$$s(t) = B\cos\omega t + m\sin\Omega t \tag{2}$$

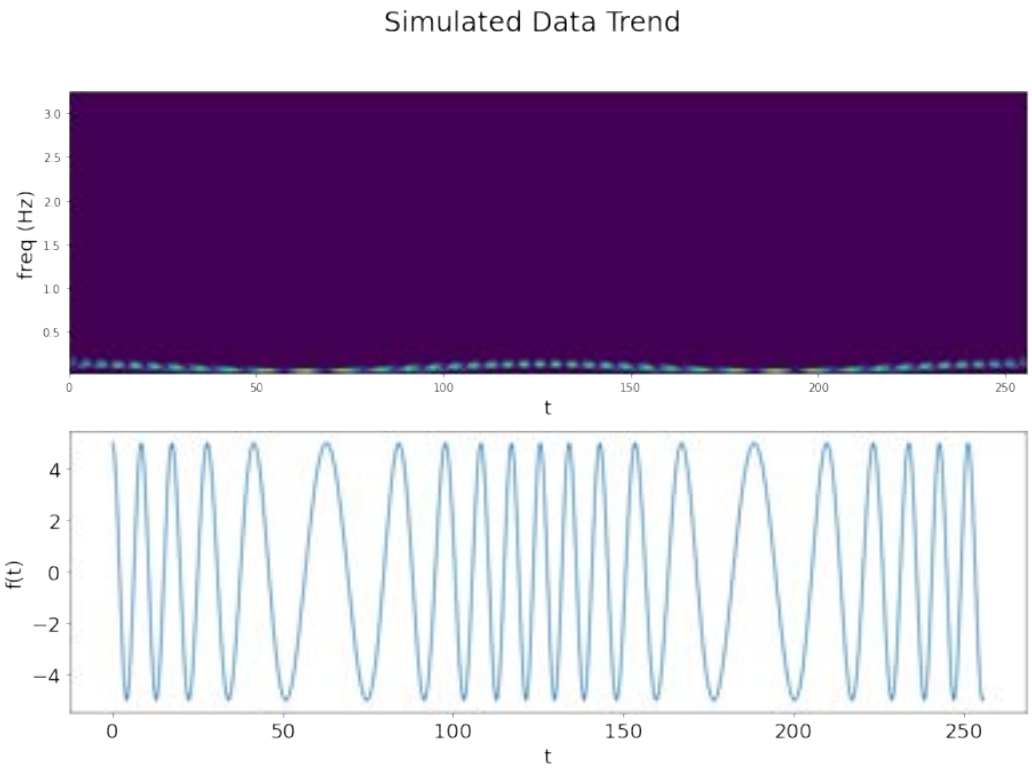

Figure 6. This image demonstrates frequency modulation. And the above one is based on wavelet transform and the below one represents raw data.

The frequency modulation signal 6 can be important if the fundamental physical properties of the climate system undergo secular changes such as the increase in atmospheric moisture due to global warming.

From the 6, we could see that the wavelet transform shows the frequency modulation very well by decomposing the frequency into different layers and it results a wave-shape line in the wavelet transform graph because the higher frequency disappear regularly.

2.2.4. ABRUPT CHANGE IN FREQUENCY

We define abrupt change in frequency as

$$s(t) = \begin{cases} C\cos\omega_1 t, & \text{if } t < 256 \\ C\cos\omega_2 t, & \text{if } t \geq 256 \end{cases} \tag{3}$$

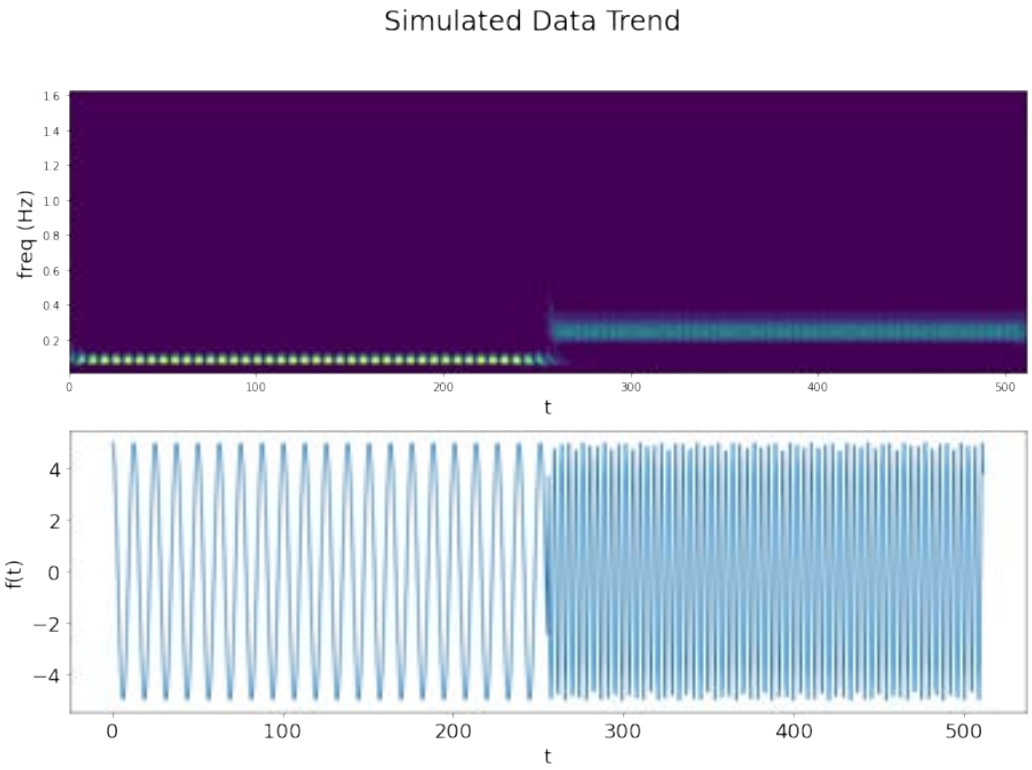

Figure 7. This image demonstrate abrupt change in frequency and the top represent wavelet transform and the bottom one represents raw data.

This is also one of the quite important climate signal associated with abrupt frequency change. This can be found in the occurrence of catastrophic event that has a long-term impact.

It is obvious that the wavelet transform captured the characteristics of data very well. There are distict difference in terms of frequency before and after the point when data has been changed dramatically.

2.2.5. ABRUPT CHANGE IN TIME

We define abrupt change in time as

$$s(t) = D\frac{t-256}{\sigma^2}\exp -\frac{(t-256)^2}{2\sigma^2} \tag{4}$$

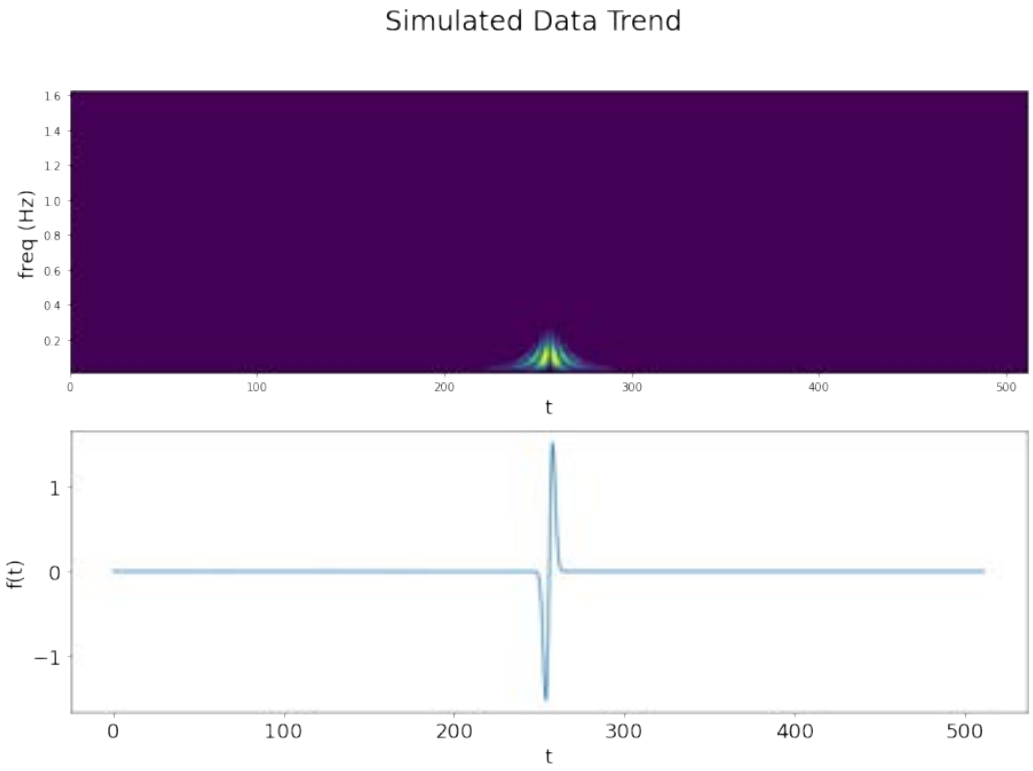

Figure 8. This image represents abrupt change in time. The top one represents wavelet transform and the bottom one represents the raw data.

In the 8, we showed a sudden change that is short and has no long-term effects. This is mostly not important from the perspective of upwelling system due to the nature of approximation using Ekman transport but it help us interpret the result wavelet transform image.

In this section, we provide examples of four most common elements of wavelet transform and it can help us interpret the data from real-world upwelling system. By decomposing a complex wavelet transform into the basic four elements, we will be able to find insights and reason the ideas unfold by the wavelet transform.

2.3. Detrend Methods

Based on 5, we find it is hard to find distinct patterns from upwelling without detrend methods because the trend will hide the changes by introducing a small frequency. In most of the literature we examined, we found they describe detrend methods as part of the denoise method and claim that it is more like art than science. However, we find that the detrend method itself might provide some important insights as well as we will be able to find aseasonal and seasonal patterns precisely.

2.3.1. Vanilla Method

In the section of Vanilla Method, we want to first address the data we utilized in this paper. In 9, the left side image represents raw data without any processing and the right side image represents nomalized data. The orange line across all six images indicates zero. We could see from the raw data that majority of the time series between $15°$ S and $21°$ S are above zero. The less positive upwelling can be viewed between $21°$ S and $36°$ S. The region below $36°$ S has much smaller upwelling in terms of magnitude and present a pronounced seasonal cycle.

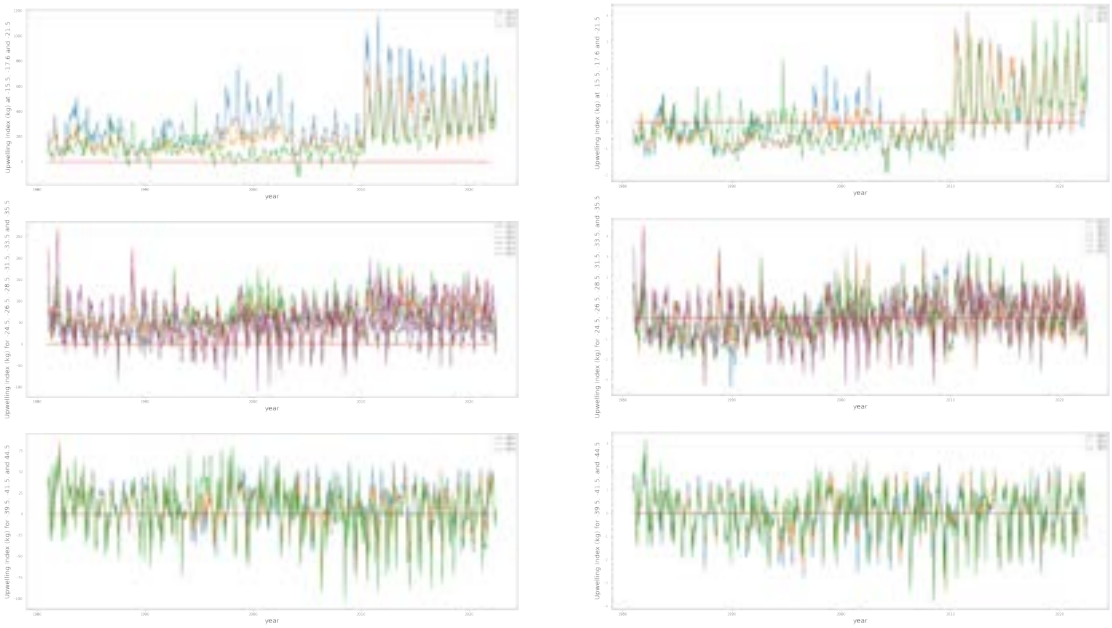

Figure 9. The left images represent raw data and the right image shows normalized data.

For the wavelet transform image, we present $15.5°$ S, $15.5°$ S, $17.5°$ S, $21.5°$ S, $24.5°$ S, $26.5°$ S, $28.5°$ S, $31.5°$ S, $33.5°$ S, $35.5°$ S, $39.5°$ S, $41.5°$ S and $43.5°$ S from left to right and from top to bottom. The wavelet analysis result will keep this pattern. One of the most interesting feature we are able to observe from the 9 is the yearly cycle. However, we can see from the original raw data, the magnitude of upwelling has been increased by a lot after 2010 which might be the consequence of finished El Nino cycle. The yearly cycle is hard to see from $15°$ S to $21°$ before 2010. There are strong multiple year cycle from $15°$ S to $21°$. The observation from other two regions accords with our reasoning from

the raw data. The year cycle is dominated between 21° S and 36° and there are more inter-yearly cycle below 36° S.

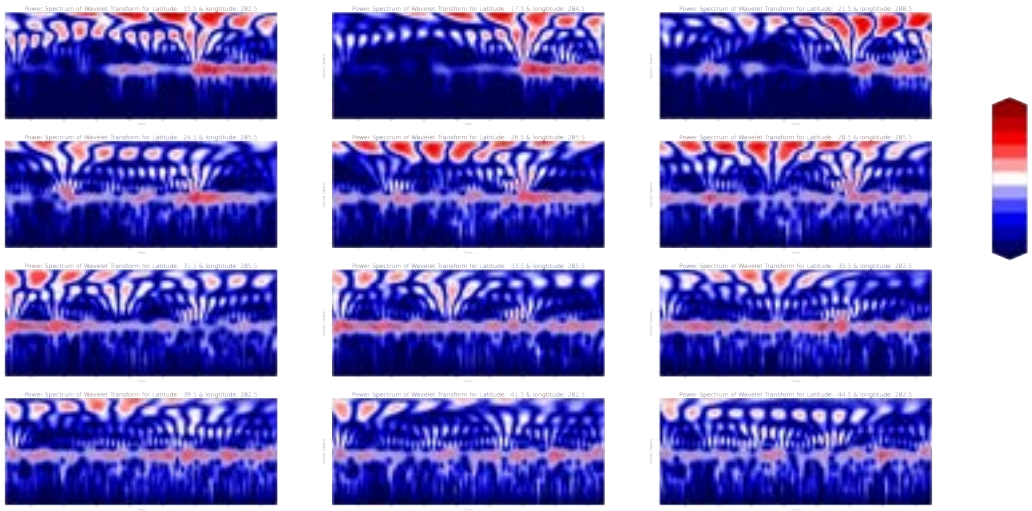

Figure 10. Wavelet transform with normalized data and each image represent one data point following the order from right to left and from top to bottom.

As a common procedure that we want to view the yearly circle using wavelet analysis, we include our results in 11. Noticed that the y-axis describe the intensity of yearly upwelling cycle across each year. The first region between 15° S and 21° show the year cycle started after 2010. This is because the intensity of upwelling cycle are too significant after 2010. This is one of the main reason we want to introduce the detrend methods.

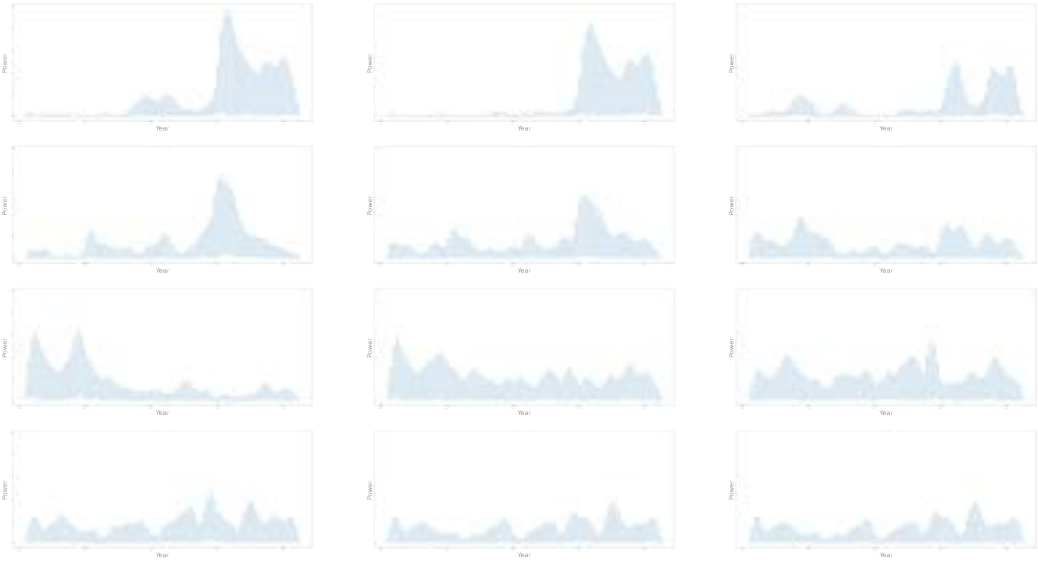

Figure 11. Yearly cycle result for each data point resulted from wavelet transform.

This is also another process that concentrate on the inter-yearly cycle (0.25 years) from wavelet analysis graph. We include the result in 12. Note that the region between 15° S and 21° and the region between

21° S and 36° has little seasonal cycle. The region below 36° S shows significant seasonal cycle. This result accords with our previous assumptions from the original raw data.

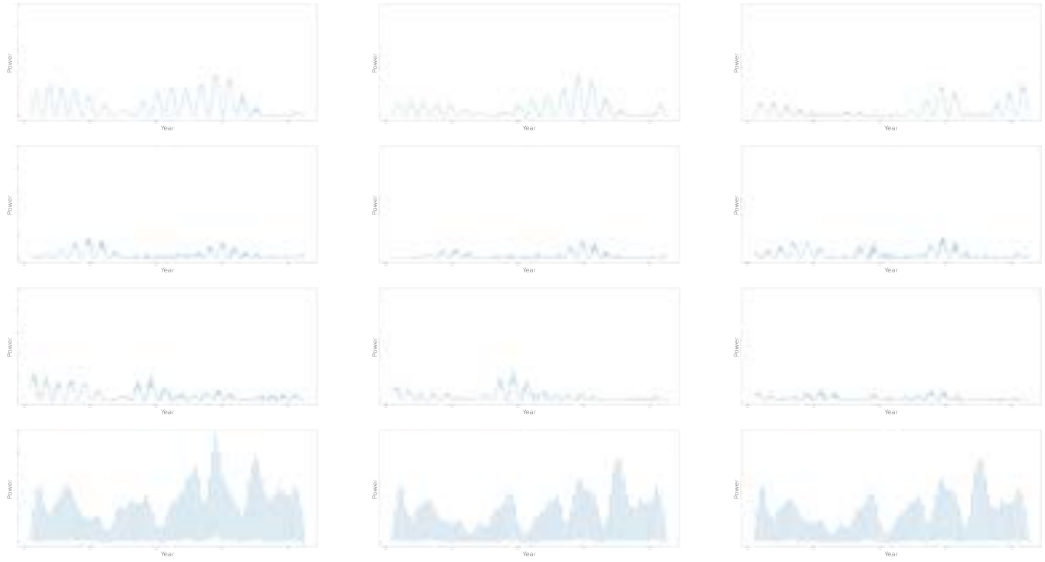

Figure 12. Seasonal cycle result for each data point resulted from wavelet transform.

This procedure has been constructed as a pipeline we utilized to analysis various time series. We have experimented with three different detrend method and we will include the results using different detrend methods about year cycle and seasonal cycles in the appendix.

2.3.2. DETREND METHOD1: CUBIC SPLINE

After we carefully review our data, the region between between 21° S and 36° has quite strong upwelling after 2010. Therefore, we want to first detrend using a nonlinear method. Therefore, cubic spline came into our consideration. The following graph 13 can demonstrate the result of normalized data using cubic spline as the detrend method.

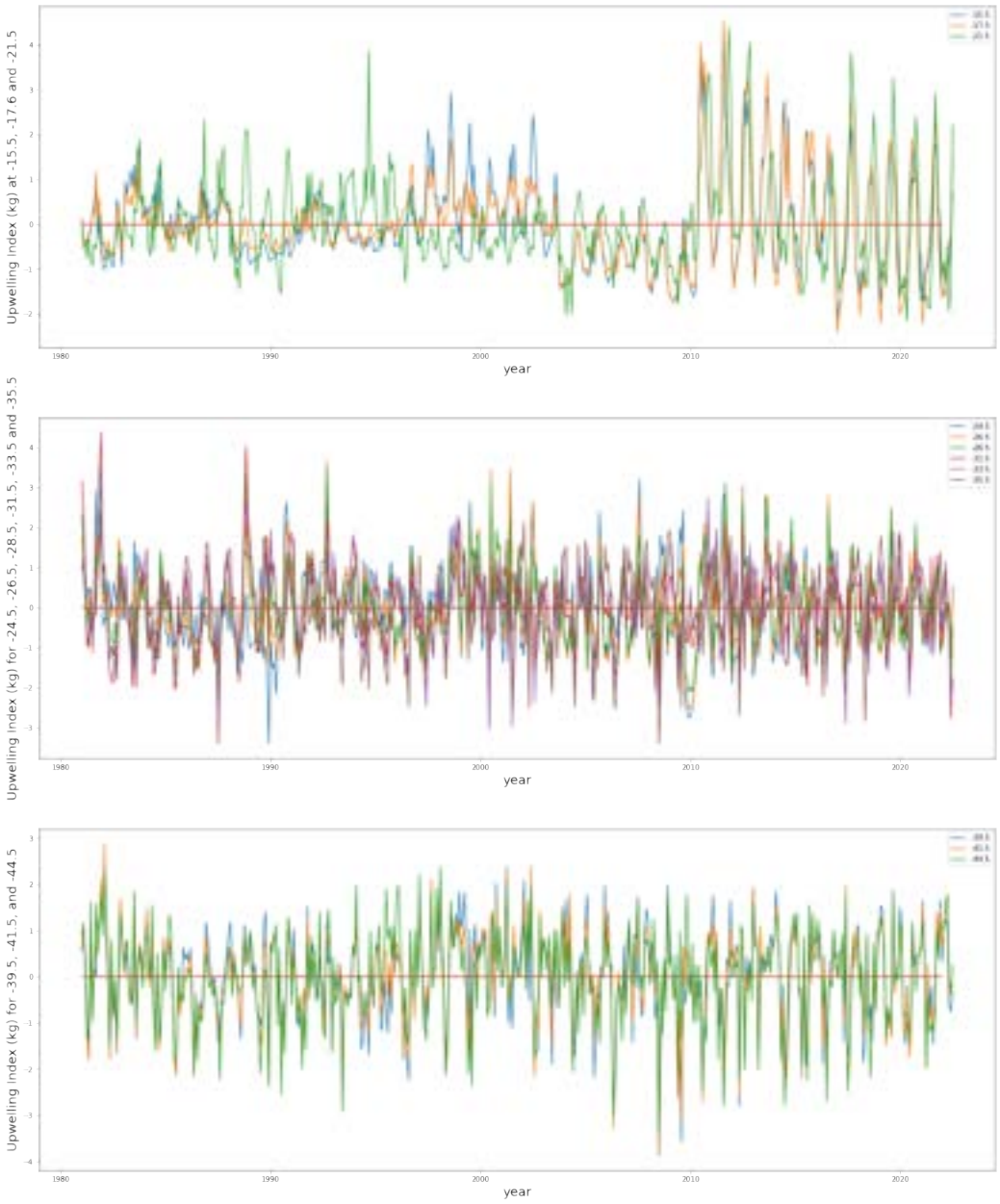

Figure 13. Cubic spline detrended data in three regions

We also include the wavelet analysis using linear regression as detrend method in 14. The result has improved but remains as vague for the first region between 21° S and 36° and also make the third region

below 36° S become harder to understand. Therefore, we include yearly cycle and inter-yearly cycle in the appendix 19 and 20.

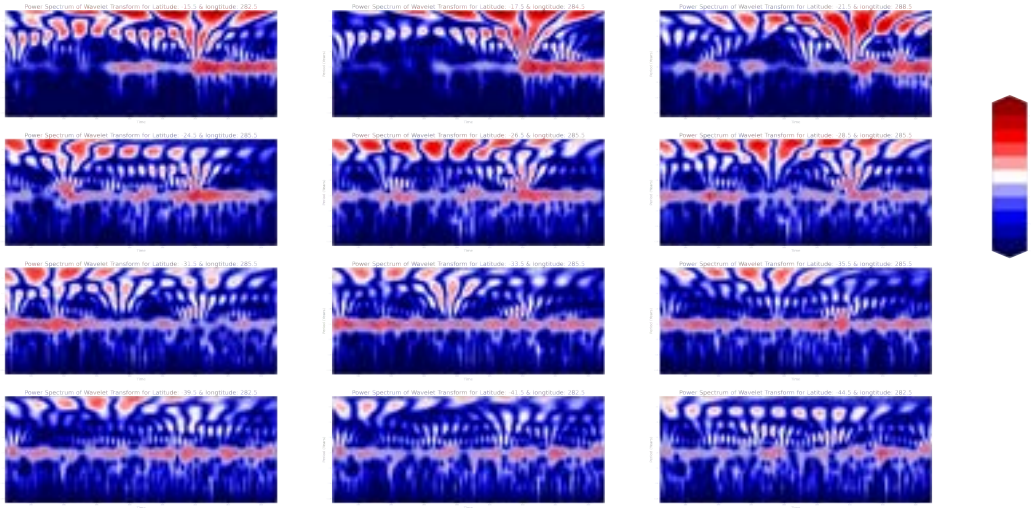

Figure 14. Wavelet Transform with cubic spline detended data and each image represent one data point following the order from right to left and from top to bottom.

2.3.3. DETREND METHOD2: LINEAR REGRESSION

Suppose we have a time series, the most nature way of detrend is subtract the time series with a linear regression of the time serie. The following graph 15 can demonstrate the result of normalized data using linear regression as the detrend method. Clearly, the linear regression detrend the time serie very well over the second region between $21°$ S and $36°$ S and the third region below $36°$. The first region between $15°$ S and $21°$ has quite strong upwelling after 2010. These data are too significant even after linear regressiond detrend.

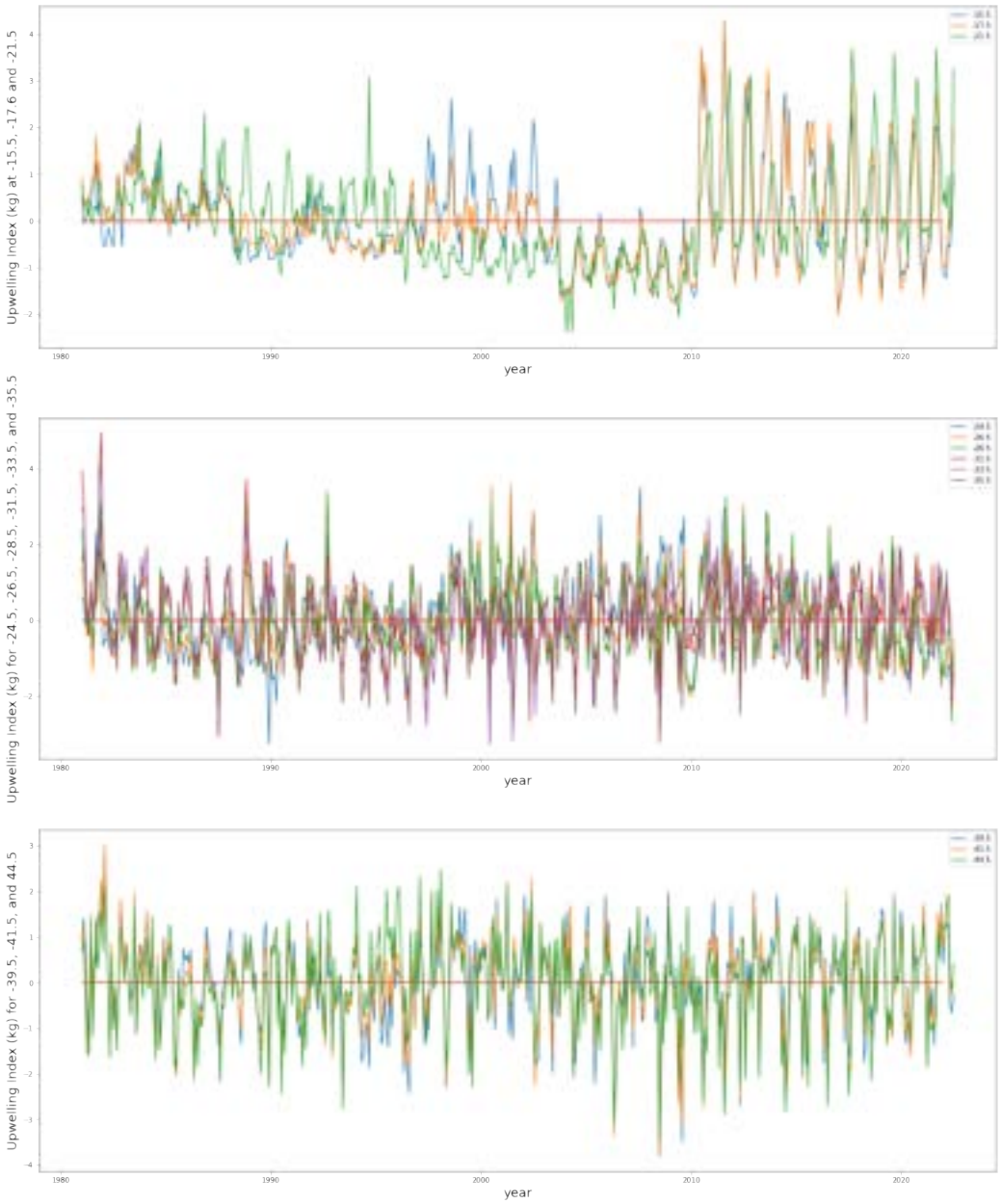

Figure 15. Linear regression detrended data in three regions

We also include the wavelet analysis using linear regression as detrend method in 21. It is obvious that the result did not alter too much from the vanilla method we discussed above. Therefore, we include yearly cycle and inter-yearly cycle in the appendix 22 and 16.

Figure 16. Yearly cycle result for each data point resulted from wavelet transform

2.3.4. DETREND METHOD3: DIFFERENCING

Then we utilized a more rigorous detrend method using differencing: $X(t) - X(t-1)$ except for the first data point. From the following 17, we could see that all of the data has been centralized. Then we are concerned whether we altered the original data too much. In other words, differencing might remove the pattern from raw data.

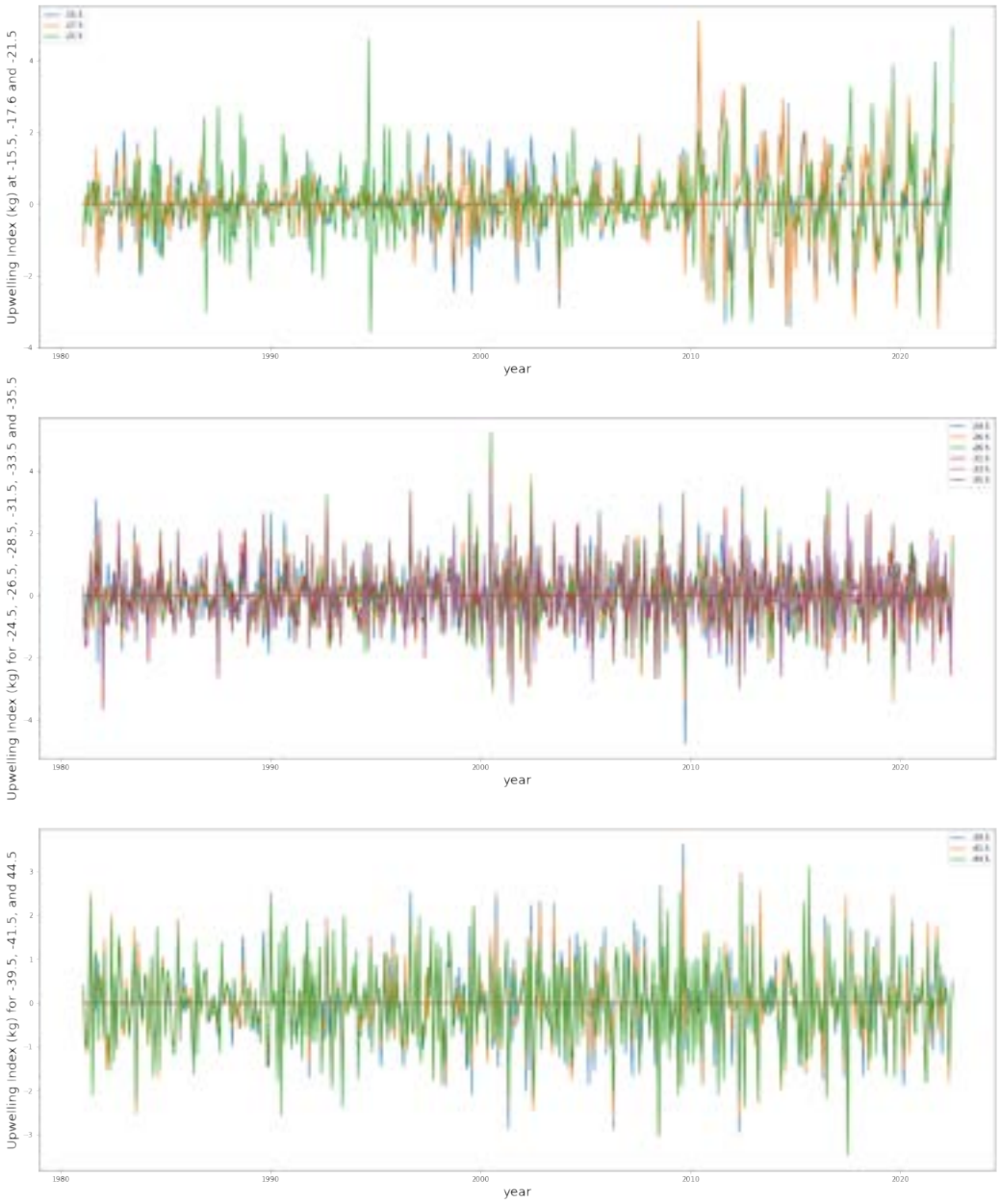

Figure 17. Differencing detrend data in three regions

Then we include the wavelet transform image in **??**. Clearly, differencing break patterns and did not help improve yearly cycle for the first region. We include yearly cycle image 23 and seasonal cycle

image 24 in the appendix. However, the differencing detrend make the seasonal cycle dramatically unstable for the first and second region that are both above 36° S.

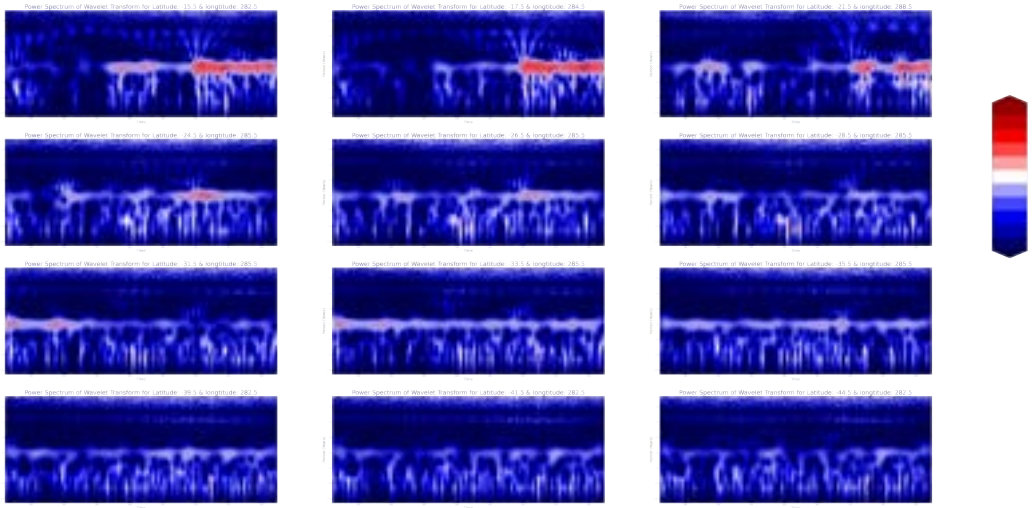

Figure 18. Wavelet Transform with differencing detended data and each image represent one data point following the order from right to left and from top to bottom.

As a conclution for the section of detrend methods, we can see that it helps to represent the pattern better using cubic spline, but designing an appropriate detrend methods can be a really hard task. With a higher order spline, we may achieve a better wavelet transform, or we can remove the patterns from the raw data entirely.

3. Discussions

During the linear regression detrend, we find the following interesting slopes for each time serie and we have included in the following table:

Latitude	Slope
15.5° S	0.69495351
17.5° S	0.64828242
21.5° S	0.50510574
24.5° S	0.05141406
26.5° S	0.05314334
28.5° S	0.08235469
31.5° S	0.06196924
33.5° S	0.06412974
35.5° S	0.01436979
39.5° S	0.0009196
41.5° S	-0.01466811
43.5° S	-0.05163849

Clearly, in the third region which below 36° S, upwelling shows no sign of increasing. However, for the Peruvian and Chilean upwelling system, one of the most interesting observation we have is that the upwelling system between 15° S and 36° S increase significantly after 2010, which worth further investigation. All of the wavelet transform results are quite useful to discuss intensity over yearly pattern or season pattern. For detrend methods, we will need to define a criteria to determine whether one detrend method should apply over time series. Otherwise, detrend methods will not help the raw data for yearly cycle and seasonal cycle.

(**?**)

References

José Arias-Pérez and Juan Tavera-Mesías. Linking knowledge management maturity and innovation in leading companies in research and development. 06 2015.

A. Bakun, B. A. Black, S. J. Bograd, M. García-Reyes, A. J. Miller, R. R. Rykaczewski, and W. J. Sydeman. Anticipated effects of climate change on coastal upwelling ecosystems. *Current Climate Change Reports*, 1(2):85–93, June 2015. ISSN 2198-6061. doi: 10.1007/s40641-015-0008-4. Funding Information: Acknowledgments We thank S.A. Thompson for editing, formatting, and referencing this paper. AJM thanks NSF for funding under grants OCE-1026607, OCE-0960770 and OCE-1419306. BAB, WJS, MGR, RRR and SJB thank NSF for funding under grant OCE-1434732. Publisher Copyright: © 2015, Springer International Publishing AG.

Andrew Bakun. Global climate change and intensification of coastal ocean upwelling. *Science*, 247 (4939):198–201, 1990. doi: 10.1126/science.247.4939.198. URL https://www.science.org/doi/abs/10.1126/science.247.4939.198.

Andrew Bakun, David B. Field, Ana Redondo-Rodriguez, and Scarla J. Weeks. Greenhouse gas, upwelling-favorable winds, and the future of coastal ocean upwelling ecosystems. *Global Change Biology*, 16(4):1213–1228, 2010. doi: https://doi.org/10.1111/j.1365-2486.2009.02094.x. URL https://onlinelibrary.wiley.com/doi/abs/10.1111/j.1365-2486.2009.02094.x.

Dante Figueroa and Carlos Moffat. On the influence of topography in the induction of coastal upwelling along the chilean coast. *Geophysical Research Letters*, 27(23):3905–3908, 2000. doi: https://doi.org/10.1029/1999GL011302. URL https://agupubs.onlinelibrary.wiley.com/doi/abs/10.1029/1999GL011302.

Bessa Ismail, Makaoui Ahmed, Hilmi Karim, and Afifi Mohamed. Wavelet analysis on upwelling index along the moroccan atlantic coast. *European Scientific Journal, ESJ*, 13(12):276, 2017.

Jochen Kaempf and Piers Chapman. *Upwelling Systems of the World*. 01 2016. doi: 10.1007/978-3-319-42524-5.

Vivian Montecino and Carina Lange. The humboldt current system: Ecosystem components and processes, fisheries, and sediment studies. *Progress In Oceanography*, 83:65–79, 12 2009. doi: 10.1016/j.pocean.2009.07.041.

N Narayan, André Paul, Stefan Mulitza, and Michael Schulz. Trends in coastal upwelling intensity during the late 20th century. *Ocean Science*, 6(3):815–823, 2010.

Ryan R Rykaczewski, John P Dunne, William J Sydeman, Marisol García-Reyes, Bryan A Black, and Steven J Bograd. Poleward displacement of coastal upwelling-favorable winds in the ocean's eastern boundary currents through the 21st century. *Geophysical Research Letters*, 42(15):6424–6431, 2015.

Daiwei Wang, Tarik C Gouhier, Bruce A Menge, and Auroop R Ganguly. Intensification and spatial homogenization of coastal upwelling under climate change. *Nature*, 518(7539):390–394, 2015.

```
Python code for data:
def upwell(ektrx, ektry, coast_angle):
  import numpy as np
  pi = 3.1415927
  degtorad = pi/180.
  alpha = (360 - coast_angle) * degtorad
  s1 = np.cos(alpha)
  t1 = np.sin(alpha)
  s2 = -1 * t1
  t2 = s1
  perp = (s1 * ektrx) + (t1 * ektry)
  para = (s2 * ektrx) + (t2 * ektry)
  return(perp/10)
\label{code}
```

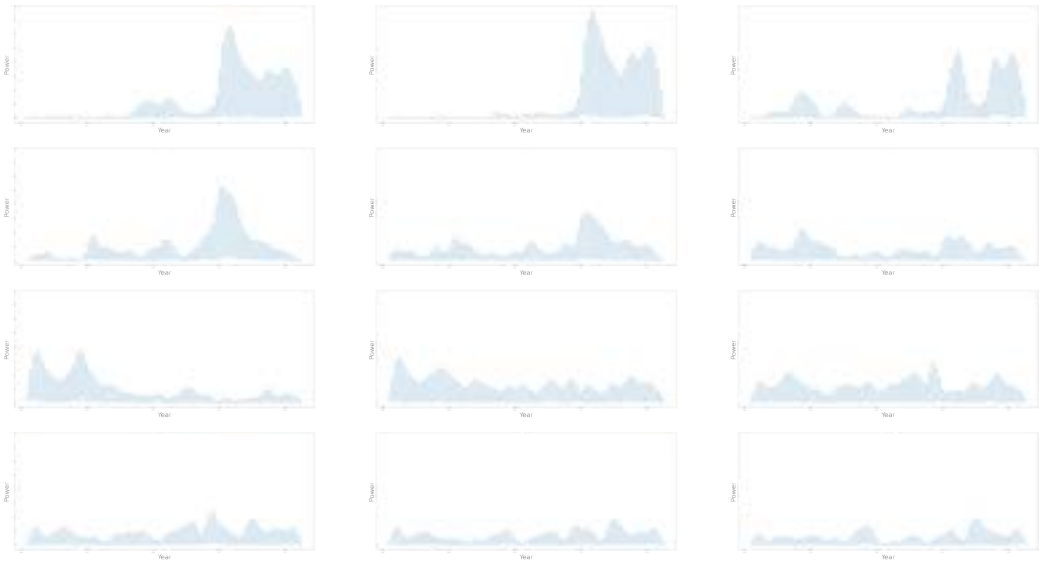

Figure 19. Yearly cycle result for each data point resulted from wavelet transform

Figure 20. Seasonal cycle result for each data point resulted from wavelet transform

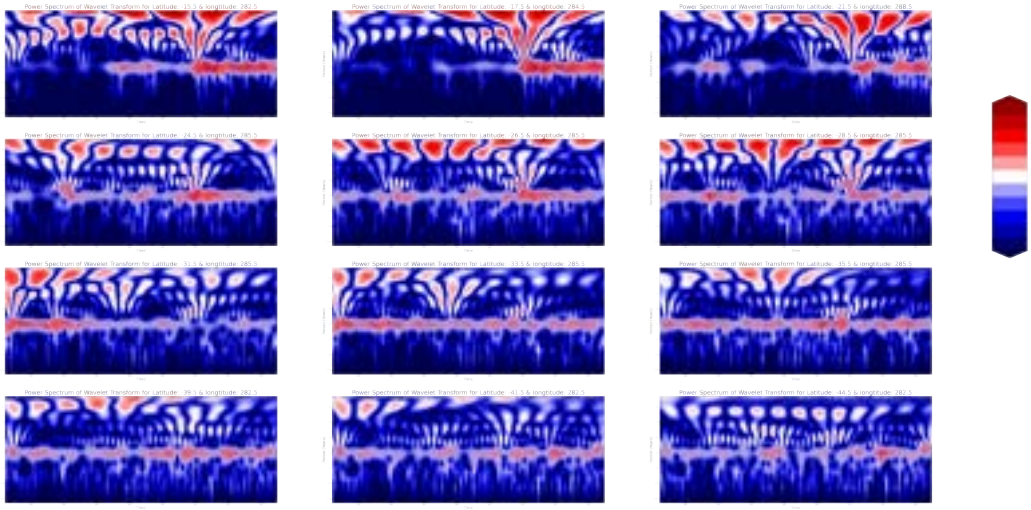

Figure 21. Wavelet Transform with linear regression detended data and each image represent one data point following the order from right to left and from top to bottom.

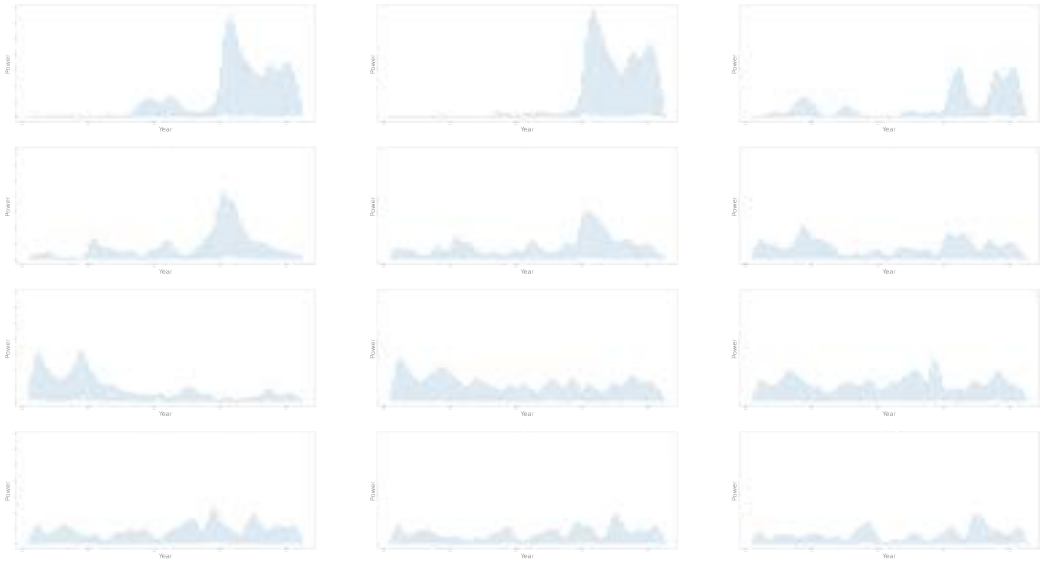

Figure 22. Yearly cycle result for each data point resulted from wavelet transform

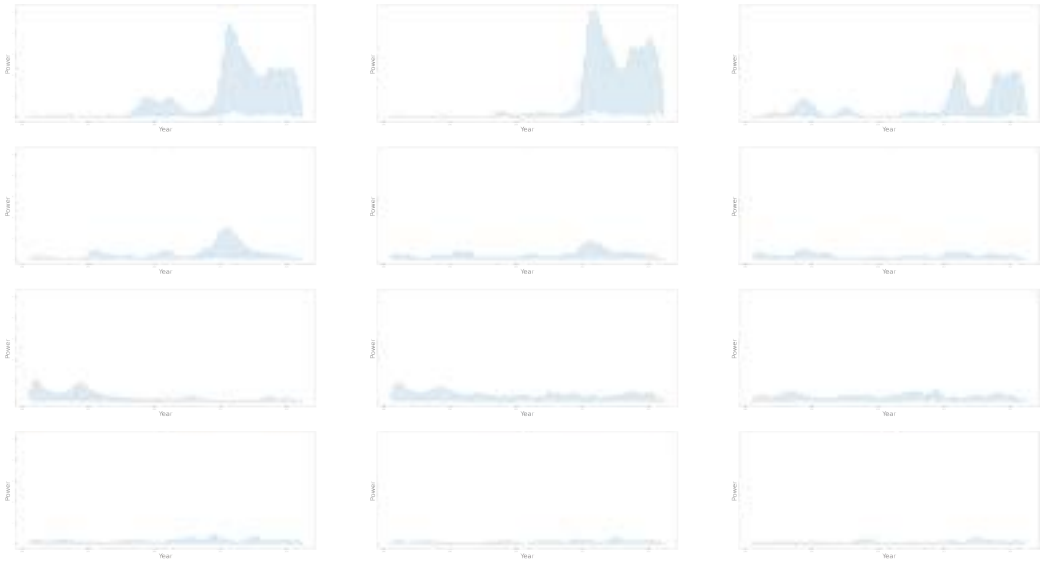

Figure 23. Yearly cycle result for each data point resulted from wavelet transform

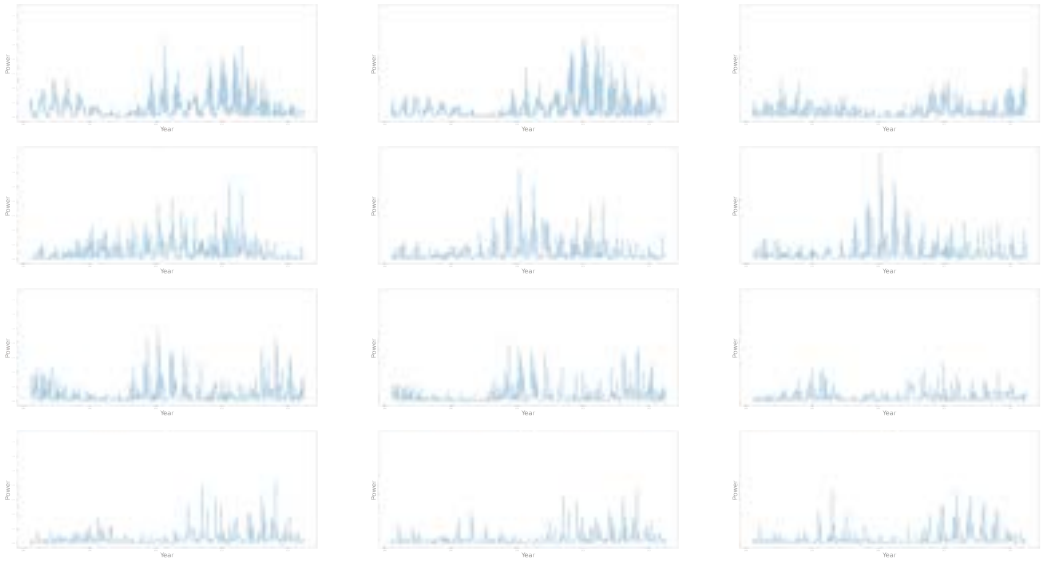

Figure 24. Seasonal cycle result for each data point resulted from wavelet transform

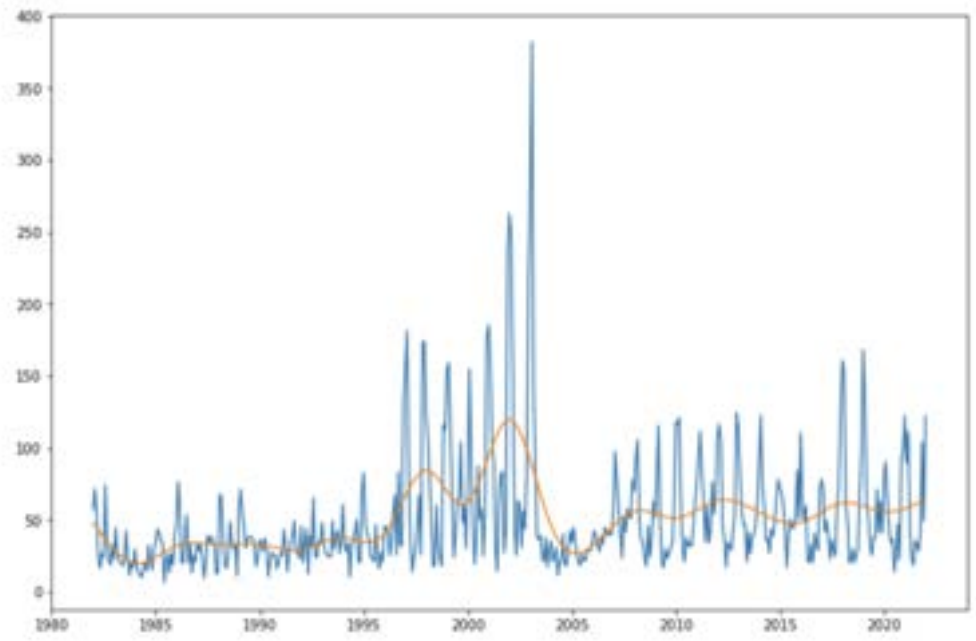

Figure 25. Morocco homogenization

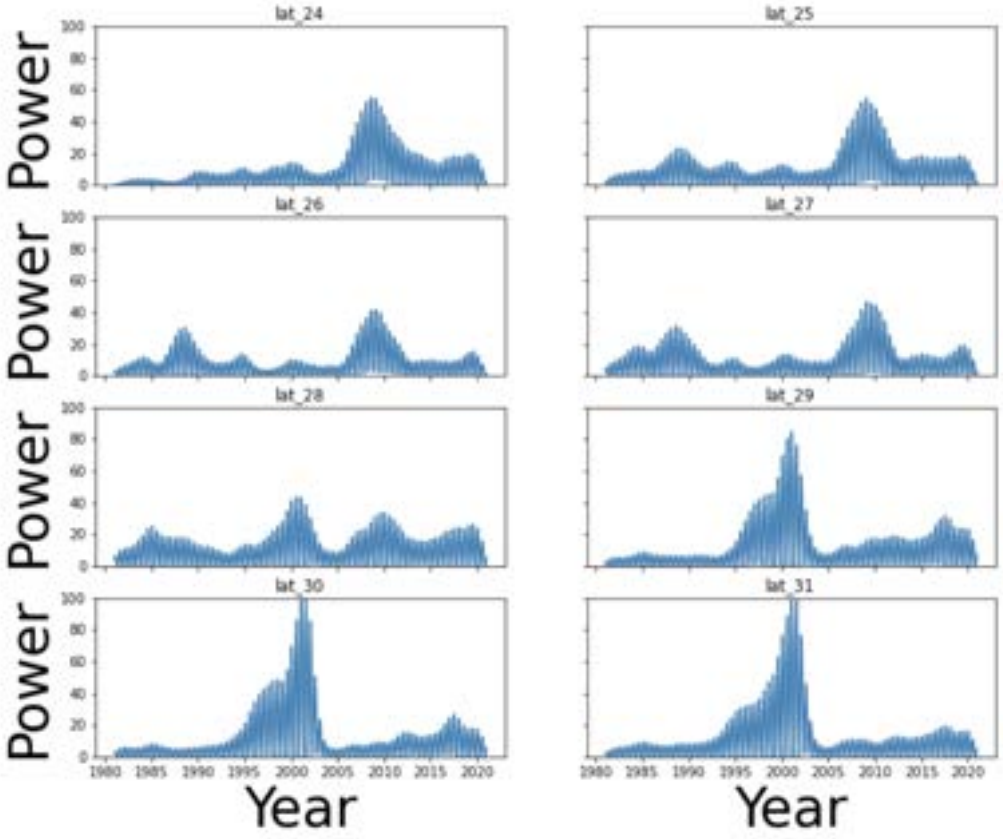

Figure 26. Morocco power graph

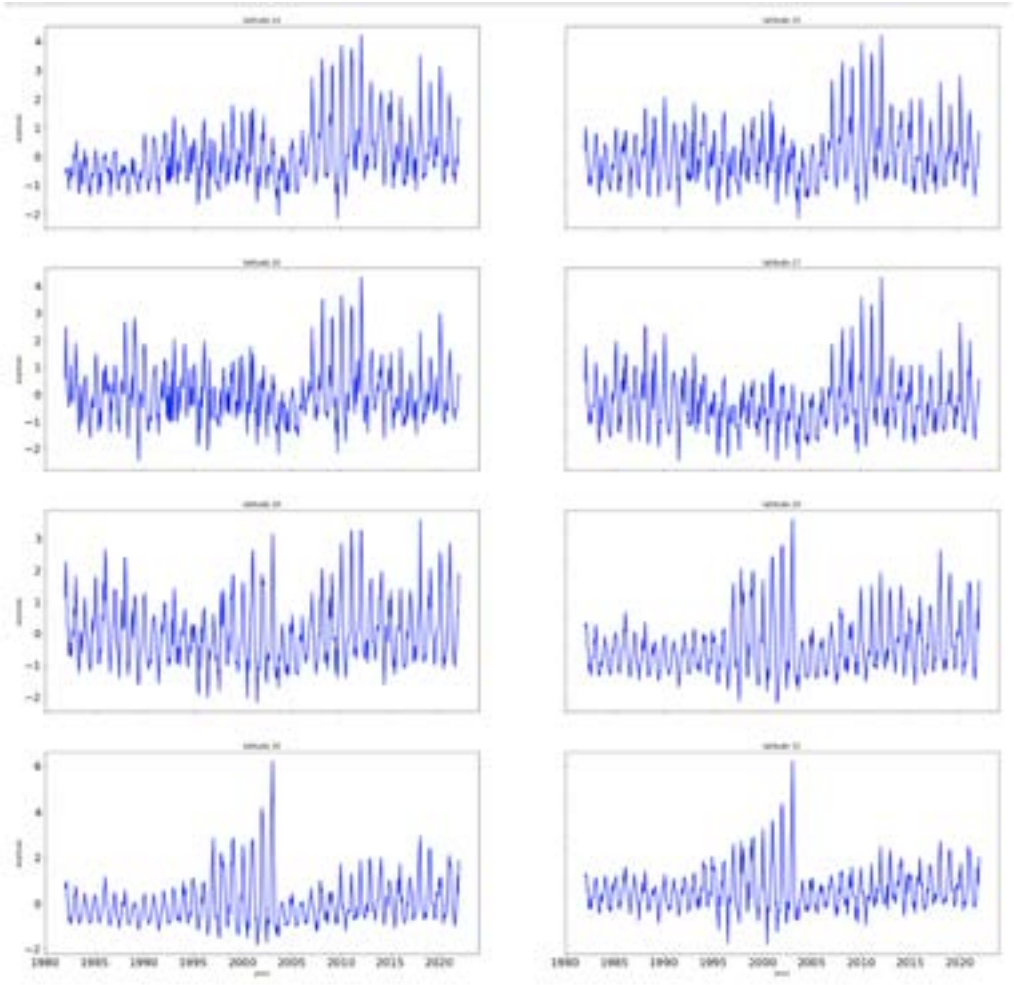

Figure 27. Morocco time series